



Analysis of air temperature dynamics in the “local climate zones” of Novi Sad (Serbia) based on long-term database from an urban meteorological network

Dragan Milošević¹ · Stevan Savić¹ · Milena Kresoja² · Zorana Lužanin³ · Ivan Šećerov¹ · Daniela Arsenović¹ · Jelena Dunjić⁴ · Andreas Matzarakis^{5,6}

Received: 14 April 2020 / Revised: 11 November 2020 / Accepted: 20 November 2020
© ISB 2021

Abstract

A comprehensive analysis of air temperature (T_a) dynamics in “local climate zones” (LCZs) of Novi Sad (Serbia) was based on measurements from 17 stations during 3 years. Hourly changes of T_a , cooling rates (CR), heating rates (HR), and urban heat island (UHI) intensity were assessed on seasonal and annual level and during heat wave (HW) and cold wave (CW) periods. Substantial differences are observed for minimum (T_{min}) and mean temperatures (T_{mean}) between LCZs. Two-phase nocturnal cooling was recognized with the first cooling phase characterized by intensive LCZ dependent cooling starting at 1–3 h before sunset and lasting until 3–4 h after sunset. The second cooling phase lasts until sunrise and is characterized by less intensive and LCZ nondependent cooling. The most intensive cooling (CR_{peak}) was observed in first cooling phase of HW and ranged from -1.6 °C h⁻¹ in street canyon (LCZ 2) to -3.9 °C h⁻¹ in forest (LCZ A). Furthermore, a new cooling indicator (CR_{total}) was introduced. Due to cooling differences, the most intensive UHI of 5.5 °C was noticed between LCZs 2 and A at sunset + 1 h during HW. Two-phase diurnal heating was also recognized in LCZs with the first heating phase characterized by intensive LCZ dependent heating starting at sunrise and lasting until 4–7 h afterwards. The most intensive heating (HR_{peak}) ranged from 2.0 °C h⁻¹ in street canyon to 3.0 °C h⁻¹ in industrial area (LCZ 8) during HW. The second heating phase lasts until sunset and is characterized by less intensive heating and smaller HR differences between LCZs.

Keywords Urban heat island · Cooling rate · Heating rate · Local climate zone · Urban meteorological network · Mid-sized city

✉ Dragan Milošević
dragan.milosevic@dgt.uns.ac.rs

¹ Climatology and Hydrology Research Centre, Faculty of Sciences, University of Novi Sad, Trg Dositeja Obradovića 3, Novi Sad 21000, Serbia

² Institute of Economic Sciences, Zmaj Jovina 12, Belgrade 11000, Serbia

³ Department of mathematics and informatics, Faculty of Sciences, University of Novi Sad, Trg Dositeja Obradovića 3, Novi Sad 21000, Serbia

⁴ Department of Geography, Tourism and Hotel Management, Faculty of Sciences, University of Novi Sad, Trg Dositeja Obradovića 3, Novi Sad 21000, Serbia

⁵ Research Centre Human Biometeorology, German Meteorological Service, Stefan-Meier-Str. 4, D-79104 Freiburg, Germany

⁶ Environmental Meteorology, Faculty of Environment and Natural Resources, Albert-Ludwigs-University Freiburg, Werthmann strasse 10, D-79085 Freiburg, Germany

Introduction

Climate relevant information for the development of healthy cities can be obtained from urban climate studies that belong to the rapidly growing scientific field (Stewart et al. 2014). Studying temporal and spatial dynamics of air temperature (T_a) on micro- and local scale can advance the understanding of urban heat island (UHI) phenomenon and the development of UHI mitigation strategies, thus contributing to healthy and comfortable cities.

Urbanization alters land cover, land use, and energy balance leading to the changes in climate of cities (Chow and Svoma 2011). UHI phenomenon is one of the most studied characteristics of urban climate (Arnfield 2003; Stewart 2011) represented by characteristic warmth of the city compared to its surroundings ($\Delta T_{urban-rural}$) (Oke et al. 2017). Substantial T_a differences can be registered within the city due to heterogeneity of surface materials, building geometry, and amount of

vegetation (Konarska et al. 2016; Unger et al. 2018). To address the inadequacies in urban-rural divisions for UHI research, Stewart and Oke (2012) developed the local climate zone (LCZ) classification system. LCZ system enables a climate-based classification of urban and rural measurement sites and their local surroundings (10^2 to 10^4 m) for T_a observations and inter-site comparisons. The system classifies urban and non-urban areas into ten “built” and seven “land cover” LCZs based on their physical properties. By using the LCZ system, UHI intensity (UHII) can be defined as T_a difference between pairs of LCZs ($\Delta T_{LCZ X - LCZ Y}$) (Stewart et al. 2014).

LCZ system was previously used to study UHI phenomenon during “ideal days” or on seasonal and annual level (Siu and Hart 2013; Alexander and Mills 2014; Lehnert et al. 2015; Fenner et al. 2014; Unger et al. 2014; Leconte et al. 2015; Leconte et al. 2017; Skarbit et al. 2017; Lehnert et al. 2018; Yang et al. 2018). Furthermore, LCZ system was applied for mapping (Unger et al. 2011; Bechtel and Daneke 2012), development of urban meteorological networks (UMNs) (Lelovics et al. 2014; Šećerov et al. 2015; Caluwaerts et al. 2020), analysis of surface temperatures (Skarbit et al. 2015; Gémes et al. 2016; Geletič et al. 2016a; Geletič et al. 2019; Gholami and Beck 2019), outdoor thermal comfort (Kovács and Németh 2012; Puliafito et al. 2013; Milošević et al. 2016; Unger et al. 2018; Kotharkar et al. 2019), urban climate modeling (Brousse et al. 2016; Geletič et al. 2016b, 2018), and urban planning (Middel et al. 2014; Perera and Emmanuel 2018). This indicates LCZ system applicability in urban climate studies.

Short-term UHI studies continue to prevail due to difficulties in collecting long-term T_a data. Among the few studies that investigated UHI during one or more years (e.g., Fenner et al. 2014; Skarbit et al. 2017; Unger et al. 2018), UMNs were the common source of data. However, only a limited number of cities have UMNs due to their complex development and maintenance (Chapman et al. 2015).

UHI genesis and development must be considered in a comprehensive analysis of this phenomenon. The UHI develops due to different cooling rates (CR) between urban and rural sites (Holmer et al. 2007), i.e., UHI effect can be noticed when rural cooling is greater than urban cooling (Oke and Maxwell 1975). However, the development of UHI is not a straight-forward process, and it happens in phases (Haeger-Eugensson and Holmer 1999; Holmer et al. 2007). Holmer et al. (2007) distinguished two cooling phases with the site-dependent cooling (phase 1) and site-nondependent cooling (phase 2). Two-phase nocturnal cooling was also observed in Montreal and Vancouver (Oke and Maxwell 1975), Singapore (Chow and Roth 2006), Göteborg (Holmer et al. 2007; Konarska et al. 2016), Adelaide (Erell and Williamson 2007), Seoul (Lee and Baik 2010), Athens (Giannopoulou et al. 2010), Phoenix (Chow and Svoma 2011), Ouagadougou (Holmer et al. 2013), Nancy (Leconte et al. 2017), and Szeged (Skarbit et al. 2017).

Cooling is one feature in the UHI development process, while the other feature is heating. When cooling stops and T_a increases after sunrise, UHI disappears due to the more intensive heating rates (HR) in rural areas than in urban areas. Accordingly, it is important to analyze HR changes for a comprehensive UHI research. Although CR are more frequently studied (e.g., Oke and East 1971; Oke and Maxwell 1975; Lee 1979; Johnson 1985; Eliasson 1994; Haeger-Eugensson and Holmer 1999; Holmer et al. 2007; Leconte et al. 2017; Skarbit et al. 2017) than HR , this study will be one of the few to investigate HR in various LCZs (e.g., Skarbit et al. 2017; Gonçalves et al. 2018; Yang et al. 2018; Yang et al. 2019).

The main goal of this study is to perform a comprehensive analysis of urban-natural and intra-urban T_a dynamics in seven LCZs of mid-sized Central European city based on 3-year database from UMN of Novi Sad (NSUNET). In order to achieve this goal, several specific objectives are defined:

- Analysis of seasonal and annual T_a in LCZs of Novi Sad. The analysis was also performed for heat wave and cold wave periods.
- Analysis of nocturnal cooling and diurnal heating on seasonal and annual level, and during heat and cold wave in various LCZs.
- Explanation of the genesis and development of hourly UHI in LCZs of a city with temperate continental climate.

Study area, data, and methods

Study area and distribution of “local climate zones”

Novi Sad is located in northern Serbia ($45^\circ 15' N$, $19^\circ 50' E$) at Pannonian Plain (80–86 m a.s.l.). Two water bodies flow through the city: Danube River and Danube-Tisa-Danube Canal (Fig. 1). South from Danube are the slopes (90–200 m a.s.l.) of low-lying Fruška Gora Mountain. Novi Sad has Cfb temperate climate (Kottek et al. 2006) with the coldest month being January with $-0.3^\circ C$ and the warmest being July with $21.8^\circ C$. The mean annual precipitation is 623 mm for the period 1949–2015 (Savić et al. 2018). The urbanized area is 112 km² with a population of 325,000.

Automated GIS method was applied to delineate LCZ types and to create LCZ map of Novi Sad (see Lelovics et al. 2014) (Fig. 1). The focus was to delineate the most typical built-up and land cover LCZs without further sub-classification. As a result, a sufficiently large LCZs (radius at least 250 m, according to Stewart and Oke 2012) and an easy to understand LCZ map was obtained (Fig. 1). Seven built-up and three land cover LCZs were recognized: compact midrise (LCZ 2), compact low-rise (LCZ 3), open midrise (LCZ 5), open low-rise (LCZ 6), large low-rise (LCZ 8), sparsely built

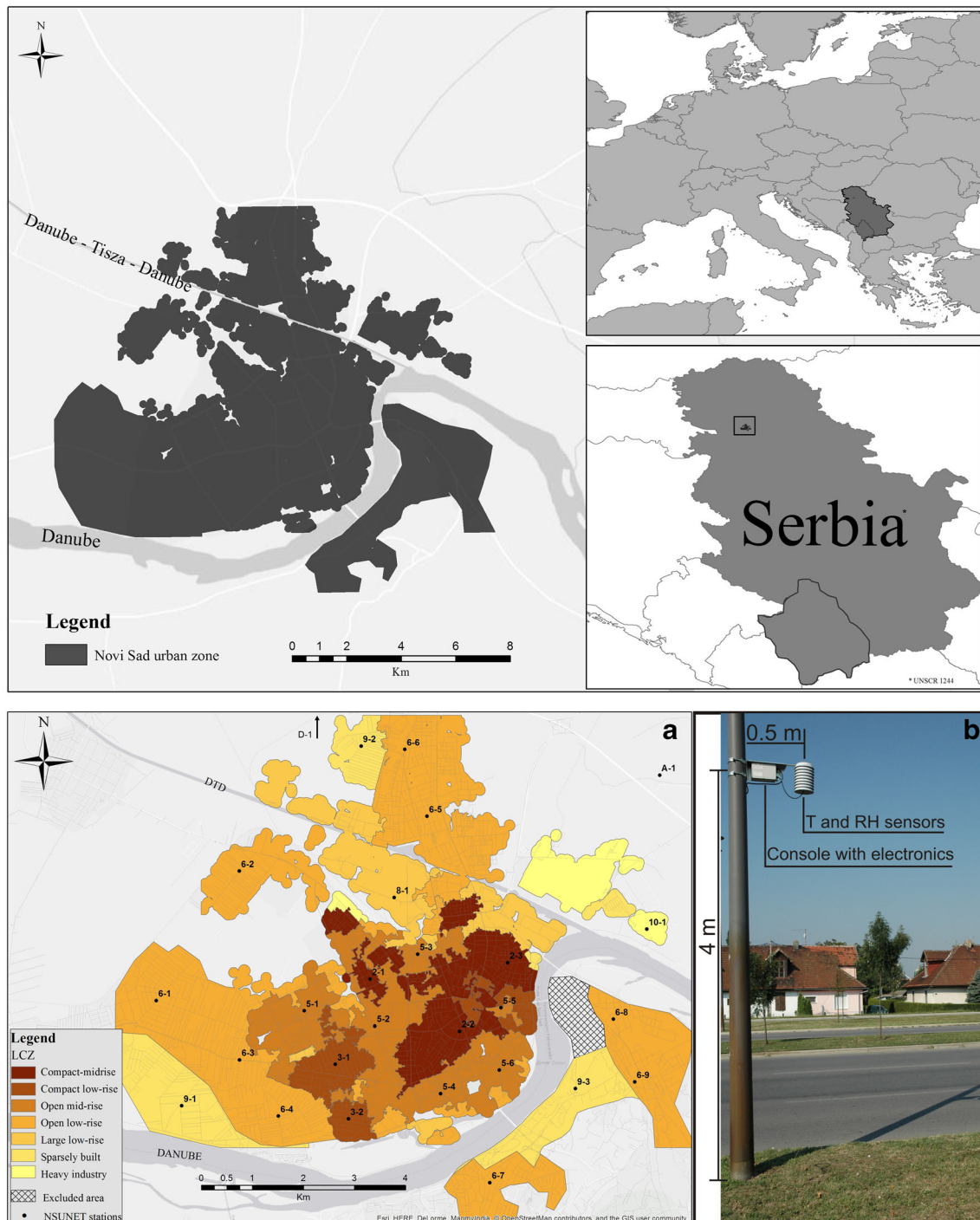


Fig. 1 Novi Sad urban zone and its location in Serbia and Europe (upper part of figure); **a** Novi Sad LCZ map with stations locations; and **b** an example of NSUNET station (lower part of figure). Note: Station name

(e.g., 6-1) consists of two numbers: the first number represents LCZ to which the station belongs (in this case it is LCZ 6), and the second number represents the station order in that zone

(LCZ 9), heavy industry (LCZ 10), dense trees (LCZ A), low plants (LCZ D), and water (LCZ G). Downtown is densely built with compact low-rise houses (LCZ 3) and midrise buildings (LCZ 2). Around downtown are residential and commercial areas with midrise buildings set in open green spaces (LCZ 5). Urban sprawl to the north, west, and south is

characterized with low-density residential housing (LCZs 6 and 9). In the northern part are located industrial areas with warehouses (LCZ 8) and heavy industry (LCZ 10). Around the city is predominant agricultural area with low plants (e.g., corn, maize) (LCZ D), and north from the city is forested area (LCZ A).

Novi Sad urban meteorological network

Novi Sad urban meteorological network (NSUNET) consists of 27 stations in various LCZs. The NSUNET was established in 2014 with twenty-five stations deployed in built-up LCZs and two stations deployed in non-urban LCZs. The main purpose of the NSUNET is to monitor diurnal, seasonal, and annual T_a and relative humidity (RH) conditions in Novi Sad at local scale (Šećerov et al. 2019). In order to ensure representative sitting of stations in LCZs, each station was placed at least several hundred meters from the LCZ border to which it belongs and at locations which micro-scale environments are representative of the local surroundings. Before stations' deployment, fieldworks were performed to find the locations that fulfilled the technical requirements regarding instruments safety, availability of electricity, and GSM signal. Multiple stations were installed in larger LCZs, while smaller number of stations was installed in smaller LCZs. Figure 1 shows stations' locations, while Table 1 shows station metadata.

NSUNET stations are equipped with T_a and RH sensors (ChipCap2) in naturally ventilated radiation screens (200×240 mm). Fully calibrated sensors are obtained from the General Electric Measurement & Control Company with the accuracy of T_a sensor of ± 0.3 °C and that of the RH sensor of $\pm 2\%$ (20–80% RH) (Šećerov et al. 2018). The sensors and accompanying equipment were connected to lamp post via 0.5-m-long arms (Fig. 1). Sensors in urban areas are located 4 m above the ground, while in rural areas they are located at 2 m above the ground. These measurement heights are in accordance with the World Meteorological Organization (WMO) guidelines (WMO 2008) and the work of Nakamura and Oke (1988) stating that T_a measured at heights of 3–5 m in urban areas are not very different from those at standard height of 2 m. Stations are activated each minute to perform measurements, and each 10 min they send the averaged 10-min readings to server. Stations use Universal Time Coordinated (UTC) synchronized with the server (Šećerov et al. 2015).

Data pre-processing and analyzed periods

Raw database included 10-min averages of 1-min T_a measurements from 27 stations for 3-year period. Due to technical problems (e.g., data transmission, vandalism), stations sometimes did not send data or they sent incorrect data (e.g., abnormally high T_a due to broken radiation shield). Five stations had over 20% of missing raw data due to the problem with data transfer (weak GSM signal) and were initially excluded from analysis.

Raw T_a data from the remaining 22 stations was pre-processed to flag outliers and unrealistic measurements. Two-step anomaly detection algorithm was developed and used in this research. The first step of the algorithm represents logical anomaly detection.

Table 1 Typical surface properties of 250-m radius environment around stations for each LCZ (obtained from Lelovics et al. 2016). Abbreviations refer to surface properties: HRE, height of roughness elements (m); SVF, sky view factor; BSF, building surface factor; ISF, impervious surface factor; PSF, pervious surface factor; ALB, albedo. Note: Low-level photo of representative location in each LCZ is given in the table. Aerial photos of representative stations are obtained from Google Earth Pro for 250-m radius environment around stations (yellow circle)

LCZ	Surface properties	Low-level photo	Aerial photo (250 m radius)
LCZ 2	HRE 16.3–20.8 SVF 0.47–0.59 BSF 0.26–0.38 ISF 0.59–0.63 PSF 0.02–0.14 ALB 0.15–0.17	Station 3-2	Station 3-2
LCZ 3	HRE 12 SVF 0.59–0.61 BSF 0.22–0.27 ISF 0.64–0.66 PSF 0.09–0.12 ALB 0.16–0.17	Station 3-2	Station 3-2
LCZ 5	HRE 15.9–25.7 SVF 0.64–0.88 BSF 0.09–0.35 ISF 0.46–0.67 PSF 0.08–0.33 ALB 0.16–0.18	Station 5-6	Station 5-6
LCZ 6	HRE 12 SVF 0.63–0.99 BSF 0.18–0.21 ISF 0.63–0.86 PSF 0.08–0.38 ALB 0.16–0.18	Station 6-4	Station 6-4
LCZ 8	HRE 12 SVF 0.84 BSF 0.31 ISF 0.47 PSF 0.23 ALB 0.17	Station 8-1	Station 8-1
LCZ 9	HRE 12 SVF 0.82 BSF 0.00–0.09 ISF 0.26–0.56 PSF 0.35–0.79 ALB 0.17–0.19	Station 9-2	Station 9-2
LCZ 10	HRE 12 SVF 0.96 BSF 0.02 ISF 0.57 PSF 0.41 ALB 0.18	Station 10-1	Station 10-1
LCZ A	HRE 0.00 SVF 1.00 BSF 0.00 ISF 0.21 PSF 0.79 ALB 0.15	Station A-1	Station A-1
LCZ 0	HRE 0.00 SVF 1.00 BSF 0.00 ISF 0.31 PSF 0.69 ALB 0.12	Station D-1	Station D-1

Let $t_i^j, i = 1, \dots, n, j = 1, \dots, 22$ denote observed T_a in time i at station j . If $t_i^j > 50^\circ\text{C}$ or $t_i^j < -30^\circ\text{C}$, then t_i^j is an outlier. In other words, temperatures exceeding 50 °C or being lower than -30 °C are considered as inaccurate, removed from dataset, and declared as missing values. The second step of the algorithm is the internal dynamic anomaly detection. In this procedure, firstly was tested whether the temperature t_i^j differs from the temperatures measured 10 min before and after time i by more than 3 °C.

That is, if $|t_i^j - t_{i-1}^j| > 3^\circ\text{C}$ and $|t_i^j - t_{i+1}^j| > 3^\circ\text{C}, i = 2, \dots, n-1, j = 1, \dots, 22$, then the measurement t_i^j was declared as critical point. Then, if t_i^j is critical point, we analyzed if t_i^j also differs by more than 3 °C from the observed temperatures of the two nearest stations. The two stations with shortest distances from station j were found via haversine formula.

Let $t_i^{k_1}$ and $t_i^{k_2}$ denote temperatures measured at time i at two closest stations from station j .

If $|t_i^j - \min_{s=1,2} t_i^{k_s}| > 3^\circ\text{C}$, the value t_i^j is removed from dataset and declared as a missing value (more details in Supplementary 1). After the pre-processing procedure, additional five stations were excluded due to numerous outliers and unrealistic measurements. The final step in the pre-processing procedure was imputation of missing value. We input missing values by means of interpolation only in cases when the gap is no longer than 1 h. In this case, maximum gap was 5 consecutive missing values.

After pre-processing, T_a from 17 stations located in six built-up and one land cover LCZ was included in statistical analysis: five stations in each of LCZs 5 and 6, three stations in LCZ 2, and one station in each of LCZs 3, 8, 9, and A. Station in LCZ A was selected as reference station because it was deployed in forest outside the urban area. This station represents dense forest on the local scale; however, on the microscale, the trees are approximately 10 m away from the station. Among the selected stations for statistical analysis, missing data was from 0 to 6% (Supplementary 2).

Statistical analysis and indices of T_a dynamics

Hourly T_a on seasonal and annual level in seven LCZs for 3-year period (1 July 2014–31 June 2017) was analyzed. We did not assess seasonality of individual years, yet the focus was on assessing the long-term temperature dynamics (i.e., during 3 years). Seasons are defined by the meteorological calendar: winter (W) (December–February), spring (Sp) (March–May), summer (Su) (June–August), and autumn (Au) (September–November). However, in order to assess the short-term temperature dynamics, the most intensive heat wave (HW) (4 to 15 August 2015) and cold wave (CW) (6 to 12 January 2017) were analyzed. During the HW, average daily wind speeds (v) were low with maximum $v < 2.5 \text{ m s}^{-1}$. Additionally, days were almost cloudless with average < 2 oktas and one precipitation day (9 mm). CW was characterized with low average $v (< 3.5 \text{ m s}^{-1})$, while the maximum average daily v reached 5.1 m s^{-1} on first day of the CW. Days were cloudy with average cloudiness of 6 oktas and with two precipitation days (5.2 mm in total). Data is from Republic Hydrometeorological Service of Serbia.

Average values of mean (T_{mean}), maximum (T_{max}), and minimum air temperatures (T_{min}) on seasonal and annual level as well as during extreme temperature periods were calculated.

T_{mean} for day $d = 7/1/2014, \dots, 6/30/2017$ and station $j = 1, \dots, 17$ is computed as average value of recorded daily 10-min temperatures $t_i^j, i = 1, \dots, n_d^j$ at station j on day d :

$$T_{\text{mean}}^{j,d} = \frac{1}{n_d^j} \sum_{i=1}^{n_d^j} t_i^j,$$

where n_d^j denotes total number of observations recorded on day d at station j . Afterwards, daily mean temperature of each LCZ $_i, i = 2, 3, 5, 6, 8, 9, A$ for day $d = 7/1/2014, \dots, 6/30/2017$ is computed by taking the average value of daily mean temperatures $T_{\text{mean}}^{j,d}$ of stations j belonging to corresponding local climate zone i :

$$T_{\text{mean}}^{i,d} = \frac{1}{|\text{LCZ}_i|} \sum_{j \in \text{LCZ}_i} T_{\text{mean}}^j,$$

where LCZ_i denotes set of all indices of stations belonging to LCZ $_i$.

T_{max} and T_{min} are obtained in the same way taking maximum and minimum values instead of the average value, respectively.

Afterwards, UHII was assessed by comparing T_{mean} of built-up LCZs with T_{mean} of LCZ A ($\Delta T_{\text{LCZ X-LCZ A}}$) in order to quantify the urban-natural temperature differences. Also, UHII between built-up LCZs ($\Delta T_{\text{LCZ X-LCZ Y}}$) was assessed in order to quantify intra-urban temperature differences. Standard deviation (SD) of T_{mean} was also calculated in order to present how variable are the values within a LCZ.

T_a and UHI dynamics were further analyzed by calculating mean hourly CR and HR , i.e., hourly T_{mean} decrease or increase over time using following formulas:

$$CR = \frac{T_{\text{mean}}}{t} \text{ and } HR = \frac{T_{\text{mean}}}{t},$$

where T_{mean} is air temperature ($^\circ\text{C}$) and t is time.

For CR analysis, cooling indicators representing the maximum (CR_{peak}) and mean cooling rates (CR_{mean}) were calculated for two cooling phases. These indicators were previously used by Konarska et al. (2016). Additionally, one new cooling indicator was defined and named *total cooling rate* (CR_{total}) representing the sum of hourly CR_{mean} in each LCZ during cooling phases. The maximum, mean, and total HR during the two-phase heating period was also calculated and named $HR_{\text{peak}}, HR_{\text{mean}},$ and HR_{total} , respectively.

Results

T_a in LCZs

Annual and seasonal T_a vary between LCZs with larger T_{min} and T_{mean} differences and smaller T_{max} differences between the classes (Table 2).

The highest T_{min} are observed in compact midrise LCZ 2, followed by open midrise LCZ 5. On the contrary, the lowest T_{min} are observed in LCZ A, followed by LCZ 9. This is the

case for all temporal scales, i.e., from annual, seasonal, to HW and CW. The largest seasonal urban-natural T_{min} difference of 3.1 °C is observed between LCZs 2 and A in spring. Inside the city, seasonal T_{min} differences are smaller, yet they can reach up to 2.0 °C between dissimilar LCZs 2 and 9 in summer. The largest T_{min} differences are noticed during CW when the street canyon in LCZ 2 registered 5.4 °C higher T_{min} than forest in LCZ A. During HW, the largest T_{min} differences are still noticed between the same zones, yet the difference is lower ($\Delta T_{LCZ\ 2 - LCZ\ A} = 4.7$ °C). Inside the city, the largest T_{min} differences occurred between LCZs 2 and 9 reaching 2.7 °C during both HW and CW (Table 2).

For T_{mean} , the highest values are noticed in midrise LCZs 2 and 5, followed by the low-rise LCZs 3 and 8. Contrarily, the lowest T_{mean} are noticed in LCZ A, followed by LCZs 9 and 6. The largest seasonal T_{mean} differences occurred between LCZs 2 and A in summer (2.0 °C). Inside the city, the largest seasonal T_{mean} differences of up to 0.9 °C were registered between LCZs 2 and 9 in spring and summer. During HW and CW, the T_{mean} differences were more pronounced and ranged from 2.1 °C during CW to 3.0 °C during HW between LCZs 2 and A. Inside the city, T_{mean} differences were smaller and reached 1.3 °C between LCZs 2 and 9 during HW and CW (Table 2).

No clear trend was detected for T_{max} differences between LCZs. It was noticed that the highest values are generally registered in low-rise LCZ 8, while the lowest are generally registered in LCZ A. However, T_{max} differences are rather small between the LCZs (Table 2).

Additional analysis was performed for SD of hourly T_{mean} between LCZs (Supplementary 3). The analysis revealed small SD differences between LCZs with the highest SD generally

registered in LCZs A and 8, and the lowest in LCZ 2. The differences in SD were higher during HW and CW then during seasons.

Cooling and heating rates in LCZs

Two-phase nocturnal cooling

Two-phase nocturnal cooling was observed in all LCZs on annual and seasonal level, and during HW and CW (Fig. 2, Supplementary 4). However, substantial cooling differences are observed between the zones.

The first cooling phase (phase 1) starts at 1–2 h before sunset in all seasons and during CW, while in summer and during HW it starts 1 h later. This phase lasts 6–7 h and ends at 3–4 h after sunset (Fig. 2 and Supplementary 4). The main features of the first cooling phase are *LCZ dependent and intensive cooling with substantial CR differences between majorities of LCZs*. These results are based on the comprehensive analysis of three CR indicators: CR_{peak} , CR_{mean} , and CR_{total} .

The most intensive CR_{peak} of -3.9 °C h⁻¹ was observed at LCZ A during HW (Fig. 2b, Supplementary 5). On the contrary, the least intensive CR_{peak} of -1.6 °C h⁻¹ was observed in LCZ 2. In between are CR_{peak} in other LCZs that ranged from -2.1 °C h⁻¹ in LCZ 5 to -3.0 °C h⁻¹ in LCZ 6 (Supplementary 5). On seasonal level, a similar situation is noticed with the most intensive CR_{peak} of -2.8 °C h⁻¹ in LCZ A and the least intensive CR_{peak} of -1.5 °C h⁻¹ in LCZs 2 and 5 during summer (Fig. 2a). It was also noticed that the highest CR_{peak} are registered between sunset + 2 h in all LCZs (Fig. 2).

Table 2 Average minimum (T_{min}), mean (T_{mean}), and maximum (T_{max}) T_a (°C) in LCZs on seasonal and annual level, and during HW and CW. Note: Red colors, the highest T_a ; green colors, the lowest T_a

Air temperature (T_a , °C)		LCZ class							Max urban-natural difference (°C)	Max intra-urban difference (°C)
		2	3	5	6	8	9	A		
T_{min}	Winter	1.1	0.1	0.7	0.0	0.1	-0.3	-1.6	2.7 _{LCZ2-A}	1.4 _{LCZ2-9}
	Spring	9.7	8.5	9.3	8.3	9.0	7.8	6.6	3.1 _{LCZ2-A}	1.9 _{LCZ2-9}
	Summer	18.8	17.8	18.3	17.4	18.0	16.8	15.9	2.9 _{LCZ2-A}	2.0 _{LCZ2-9}
	Autumn	10.2	9.1	9.8	9.0	9.0	8.6	7.5	2.7 _{LCZ2-A}	1.6 _{LCZ2-9}
	Annual	10.0	8.8	9.4	8.7	9.0	8.2	7.1	2.9 _{LCZ2-A}	1.8 _{LCZ2-9}
	Heat wave	22.7	20.9	21.8	20.7	21.1	20.0	18.0	4.7 _{LCZ2-A}	2.7 _{LCZ2-9}
	Cold wave	-10.8	-11.3	-11.3	-11.9	-12.4	-13.5	-16.2	5.4 _{LCZ2-A}	2.7 _{LCZ2-9}
T_{mean}	Winter	3.6	3.2	3.4	3.1	3.1	2.7	2.0	1.6 _{LCZ2-A}	0.9 _{LCZ2-9}
	Spring	15	14.7	14.9	14.6	15.1	14.2	13.4	1.7 _{LCZ2-A}	0.9 _{LCZ2-9}
	Summer	24.1	23.8	23.9	23.5	23.9	23.2	22.1	2.0 _{LCZ2-A}	0.9 _{LCZ2-9}
	Autumn	13.8	13.6	13.6	13.3	13.3	13.2	12.2	1.6 _{LCZ2-A}	0.6 _{LCZ2-9}
	Annual	14.4	14.2	14.3	13.9	13.7	13.7	12.7	1.7 _{LCZ2-A}	0.7 _{LCZ2-8,9}
	Heat wave	29.0	28.4	28.7	28.2	28.5	27.7	26.0	3.0 _{LCZ2-A}	1.3 _{LCZ2-9}
	Cold wave	-7.7	-7.9	-7.9	-8.1	-8.4	-9.0	-9.8	2.1 _{LCZ2-A}	1.3 _{LCZ2-9}
T_{max}	Winter	7.3	7.5	7.3	7.5	7.4	7.0	6.9	0.6 _{LCZ3,6-A}	0.5 _{LCZ3,6-9}
	Spring	19.5	19.7	19.5	19.7	20.1	19.5	19.4	0.7 _{LCZ2-A}	0.6 _{LCZ2-9}
	Summer	29.8	29.9	29.5	29.8	30.2	29.4	29.6	0.6 _{LCZ2-A}	0.8 _{LCZ2-9}
	Autumn	18.2	18.6	18.2	18.5	18.5	18.4	18.0	0.6 _{LCZ2-A}	0.4 _{LCZ2-2,5}
	Annual	18.7	18.9	18.6	18.8	19.1	18.6	18.5	0.6 _{LCZ2-A}	0.5 _{LCZ2-8,9}
	Heat wave	36.3	36.1	35.7	36.3	36.4	35.6	36.4	0.0 _{LCZ2-A}	0.8 _{LCZ2-9}
	Cold wave	-4.9	-4.9	-4.9	-4.9	-5.0	-5.3	-5.5	0.6 _{LCZ2,3,6-A}	0.4 _{LCZ2,3,6-9}

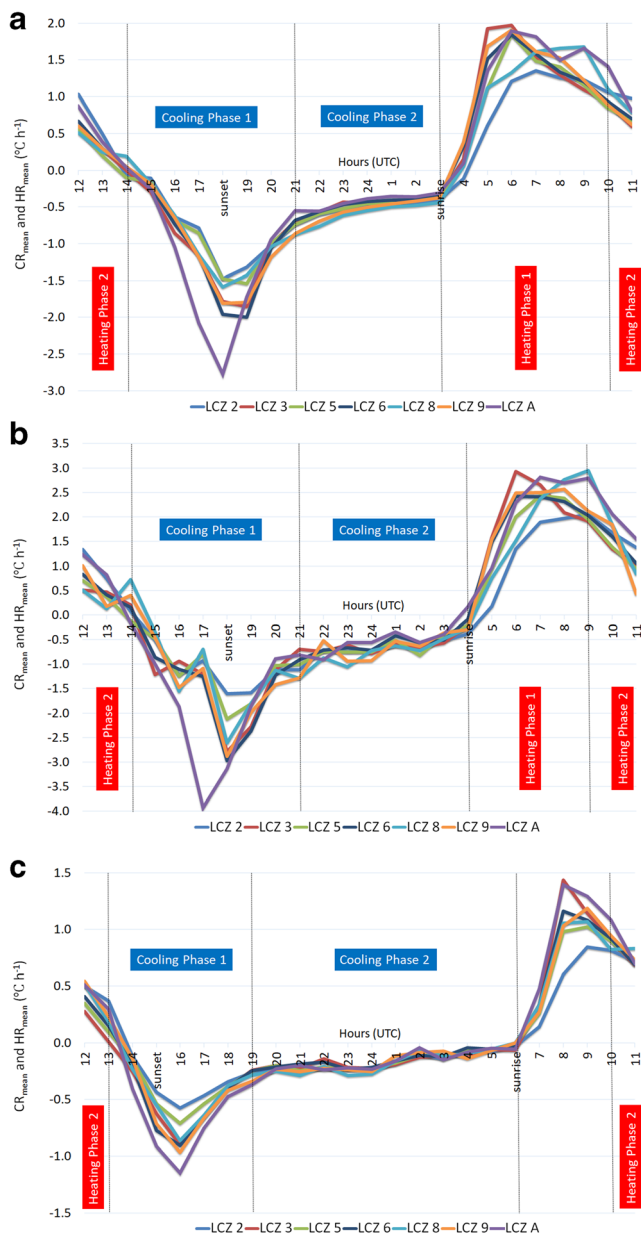


Fig. 2 Two-phase nocturnal cooling ($^{\circ}\text{C h}^{-1}$) and two-phase diurnal heating ($^{\circ}\text{C h}^{-1}$) in LCZs of Novi Sad (Serbia) during **a** summer, **b** heat wave, and **c** winter

CR_{mean} varied slightly between LCZs with noticed increase from LCZ 2 towards LCZs 5 and 8, followed by LCZs 3, 6, and 9, and reaching the highest values in LCZ A (Supplementary 5).

The most noticeable cooling differences between LCZs were observed when analyzing their total cooling (CR_{total}). The largest CR_{total} was observed outside the city (at LCZ A) during cooling phase 1 of the HW and reached -13.5°C . On the contrary, the lowest CR_{total} was observed inside an urban canyon (LCZ 2) and reached -8.1°C . Other zones had CR_{total} ranging from -8.5°C (LCZ 5) to -10.7°C (LCZ 6) (Fig. 3, Supplementary 5).

The second cooling phase (phase 2) starts at 4–5 h after sunset and ends at sunrise in all LCZs during the investigated periods. However, the duration of this phase varies between the seasons (6–7 h in warmer seasons, 10–11 h in colder seasons) due to the different night length. The main features of the second cooling phase are *LCZ independent and less intensive cooling with smaller CR differences between LCZs*.

The CR differences between the zones are small on seasonal and annual level, while they slightly increase during HW (Fig. 3, Supplementary 5). Generally, it was observed that the cooling is gradually decreasing through the night until the sunrise (Fig. 2).

Two-phase diurnal heating

Two-phase diurnal heating was generally noticed in all LCZs during all investigated periods (Fig. 2, Supplementary 4). Furthermore, different HR are observed between LCZs.

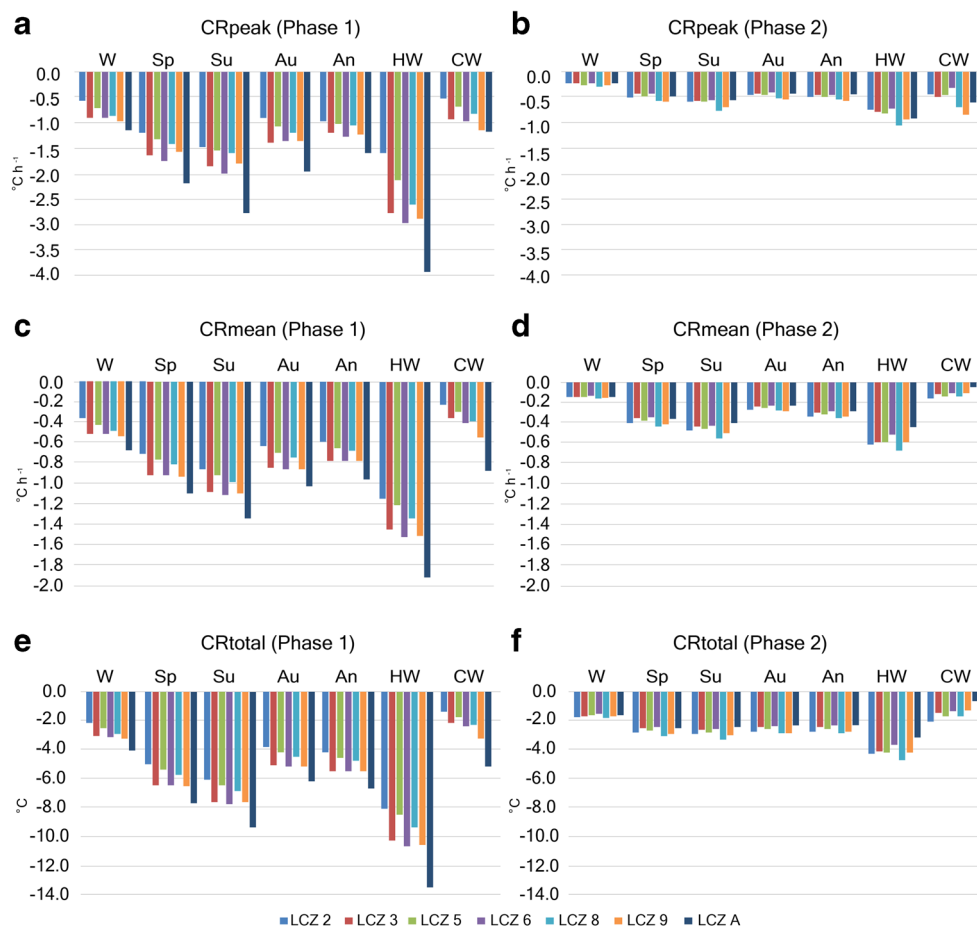
The first heating phase (phase 1) starts at sunrise and lasts from 4 to 5 h during colder seasons to 6 to 7 h during warmer seasons. The main features of the first heating phase are *LCZ dependent and intensive heating with substantial HR differences between majorities of LCZs*.

The most intensive heating (HR_{peak}) of $3.0^{\circ}\text{C h}^{-1}$ was observed in large low-rise zone (LCZ 8) during HW. At the same time, the least intensive HR_{peak} of $2.0^{\circ}\text{C h}^{-1}$ was observed in urban street canyon (LCZ 2). Other built-up zones heated up at rates between $2.4^{\circ}\text{C h}^{-1}$ (LCZs 5 and 6) and $2.9^{\circ}\text{C h}^{-1}$ (LCZ 3), while HR_{peak} reached $2.8^{\circ}\text{C h}^{-1}$ in natural LCZ A (Supplementary 6). The most intensive heating on seasonal level was observed in LCZ A and in low-rise LCZs 3 and 8, while the least intensive heating was observed in LCZ 2. The most intensive seasonal HR_{peak} reached 2°C h^{-1} in LCZ A (in spring) and in LCZ 3 (in summer). On the contrary, the least intensive summer HR_{peak} was observed in LCZ 2 ($1.4^{\circ}\text{C h}^{-1}$) (Fig. 4, Supplementary 6).

The smallest differences in HR were observed when comparing HR_{mean} between the zones. However, a clear tendency is noticed with the highest HR_{mean} observed in LCZ A and the lowest HR_{mean} observed in LCZ 2. Seasonal and annual HR_{mean} differences between these zones were approximately $0.4\text{--}0.5^{\circ}\text{C h}^{-1}$, and they slightly increased during CW and HW period (Supplementary 6).

The most noticeable heating differences between the majority of LCZs were observed when analyzing their total heating (HR_{total}). The highest HR_{total} was observed outside the city (LCZ A) during heating phase 1 of HW and reached $11.6^{\circ}\text{C h}^{-1}$. At the same time, the lowest HR_{total} was observed in urban street canyon (LCZ 2) and reached $7.5^{\circ}\text{C h}^{-1}$. Other built-up zones had HR_{total} from $9.7^{\circ}\text{C h}^{-1}$ (LCZ 5) to $11.2^{\circ}\text{C h}^{-1}$ (LCZs 3 and 9) (Fig. 4, Supplementary 6). In general, a clear trend can be detected with the smallest

Fig. 3 CR_{peak} (a, b), CR_{mean} (c, d), and CR_{total} (e, f) during cooling phase 1 and phase 2 in LCZs of Novi Sad on seasonal, annual level, and during HW and CW. Note: Values on y-axis are the same for phase 1 and phase 2 to visually better represent the substantial differences in CR between phases



HR_{total} registered in compact street canyons of LCZ 2, followed by higher HR_{total} in open midrise LCZ 5 and low-rise LCZs 3, 6, and 8, with the highest HR_{total} registered in sparsely built LCZ 9 and in LCZ A outside the city.

The second heating phase (phase 2) starts at 5–6 h after sunrise during colder seasons and at 7–8 h during warmer seasons. This heating phase duration varies between the seasons and lasts until sunset. Main features of the second heating phase are *LCZ nondependent and less intensive heating with smaller HR differences between LCZs*.

Differences in heating indicators (HR_{peak} , HR_{mean} , and HR_{total}) are small between LCZs during phase 2 on seasonal and annual level, while they slightly increase for HR_{total} during HW (Fig. 4, Supplementary 6). The highest HR_{total} was observed in LCZ 2 which stands in contrast to heating phase 1 when this zone had the lowest total heating (Supplementary 6).

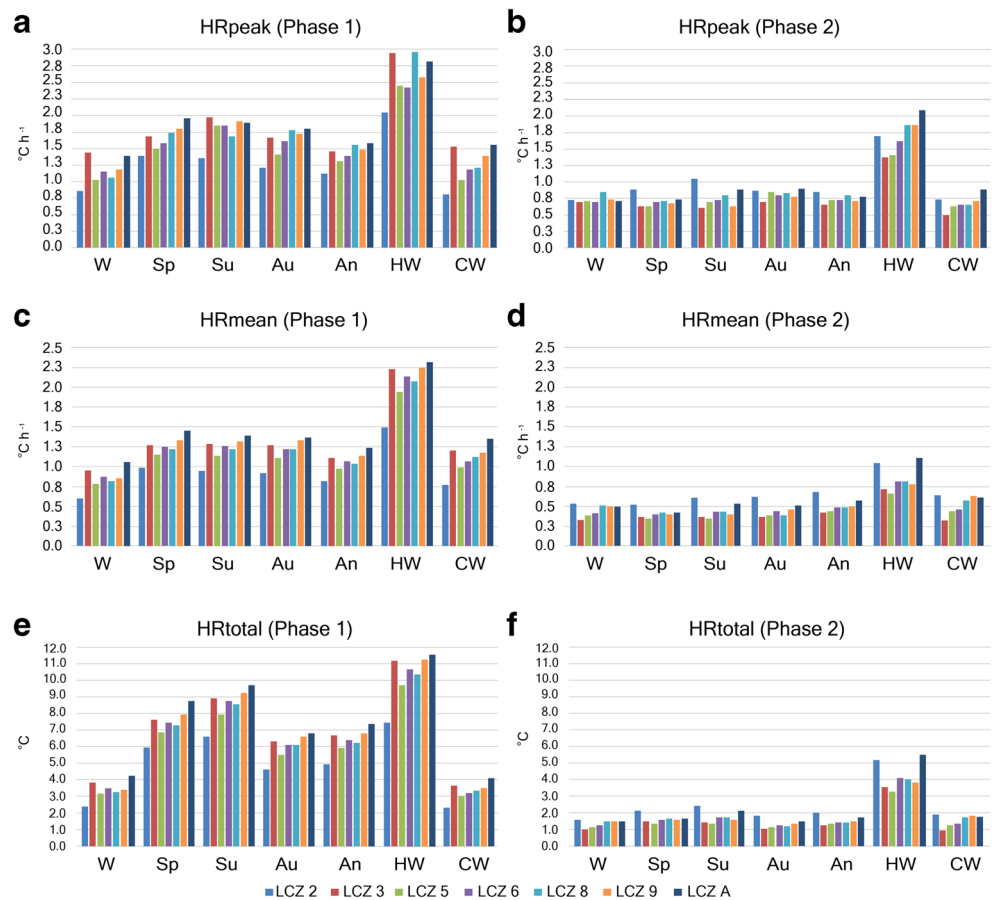
UHI genesis and hourly dynamics

UHI genesis and hourly dynamics of T_{mean} in the LCZs of Novi Sad are analyzed. For this purpose, hourly temperatures in six built-up LCZs are compared to temperatures in

natural LCZ A in order to reveal UHI intensities ($\Delta\text{UHII} = T_{\text{meanLCZx}} - T_{\text{meanLCZA}}$).

Following sunrise, hourly T_{mean} starts to increase and to converge towards similar values in LCZs (Fig. 5). Nevertheless, the highest daytime hourly T_{mean} were observed in low-rise LCZs 3 and 6, while the lowest T_{mean} were observed in LCZs A and 9. At 1–2 h before sunset, temperature in natural LCZ A starts to substantially differ from built-up LCZs, while the temperature differences between the built-up zones remain small (Fig. 5). As the night progresses, a clear inter-class LCZ pattern is noticed with the highest temperatures in urban street canyons of LCZ 2 and the lowest temperatures in natural LCZ A. Furthermore, it is generally noticed that the second warmest class is LCZ 5 and the second coldest is LCZ 9 during the nighttime period. Interesting nighttime temperature dynamics occur between low-rise LCZs. In winter and autumn, similar nighttime temperatures are noticed between low-rise LCZs 3, 6, and 8. However, this is not the case in spring and summer nighttime when temperatures in large low-rise LCZ 8 are more similar to temperatures in open midrise LCZ 5 and less similar to temperatures in other low-rise LCZs (Fig. 5).

Fig. 4 HR_{peak} (a, b), HR_{mean} (c, d), and HR_{total} (e, f) during phase 1 and phase 2 of diurnal heating in LCZs of Novi Sad on seasonal, annual level, and during HW and CW. Note: Values on y -axis are the same for phase 1 and phase 2 to visually better represent the substantial differences in HR between phases



The development of noticeable UHI starts at 1–3 h before sunset and reaches its highest intensity at sunset or between sunset and 3 h afterwards. This represents the UHI “cliff” due to its visual appearance of UHII line rising sharply and almost vertical during all investigated periods (Fig. 5). The most intensive UHI “peak” of 5.5 °C (4.1 °C) was noticed in urban street canyon (LCZ 2) during HW (CW) (Fig. 5, Supplementary 7). On seasonal level, the most intensive UHI “peak” of 3.9 °C is noticed in LCZ 2 during summer, while in winter it decreased to 2.1 °C. The second highest UHI “peak” is observed in LCZ 5 during colder seasons and in LCZ 8 during warmer seasons. UHI intensity is decreasing towards the low-rise LCZs 3 and 6 and reaches the smallest value in sparsely built LCZ 9.

A nocturnal UHI “plateau” can be observed during 10–12 h in all built-up zones (Fig. 5, Supplementary 7). Furthermore, it was noticed that the UHI “plateau” is stable in colder seasons, while it slowly decreases towards the sunrise in warmer seasons and during HW and CW. Following sunrise, the UHI “plateau” quickly vanishes, and UHI intensity sharply decreases to < 1 °C (Fig. 5). The fastest UHI intensity decrease is observed in LCZs 2 and 8 due to the lowest heating rates in these zones. As the day progresses, the UHI intensities increase again in the

afternoon towards the sunset due to higher heating rates in urban area when compared to the forest of LCZ A.

Additional analysis of the daytime and nighttime mean UHI intensity revealed a clear annual trend with nocturnal UHII decrease in the following order: LCZ 2 > LCZ 5 > LCZ 8 > LCZ 3 > LCZ 6 > LCZ 9. For example, the annual mean nocturnal UHII ranged from 1.1 °C (LCZ 9) to 2.6 °C (LCZ 2) (Table 3). Urban street canyons of LCZ 2 also show the highest seasonal nocturnal mean UHII with maximum value of 3.5 °C in summer and minimum value of 2.1 °C in winter (Table 3). During daytime, the most intensive mean UHI is observed in compact low-rise (LCZ 3) with the highest UHII in summer (1.4 °C) and during HW (1.7 °C) (Table 3).

Discussion

Results showed that the majority of LCZs have distinct T_a . The largest differences occur between LCZs 2 and A during extreme temperature events and in warmer seasons. Inside the city, temperature differences are pronounced between dissimilar LCZs (e.g., LCZ 2 and 6) while negligible between similar LCZs (e.g., LCZs 3 and 6). Annual T_{mean} differences between LCZs 2 and A reach 1.7 °C (Table 2) with smaller annual

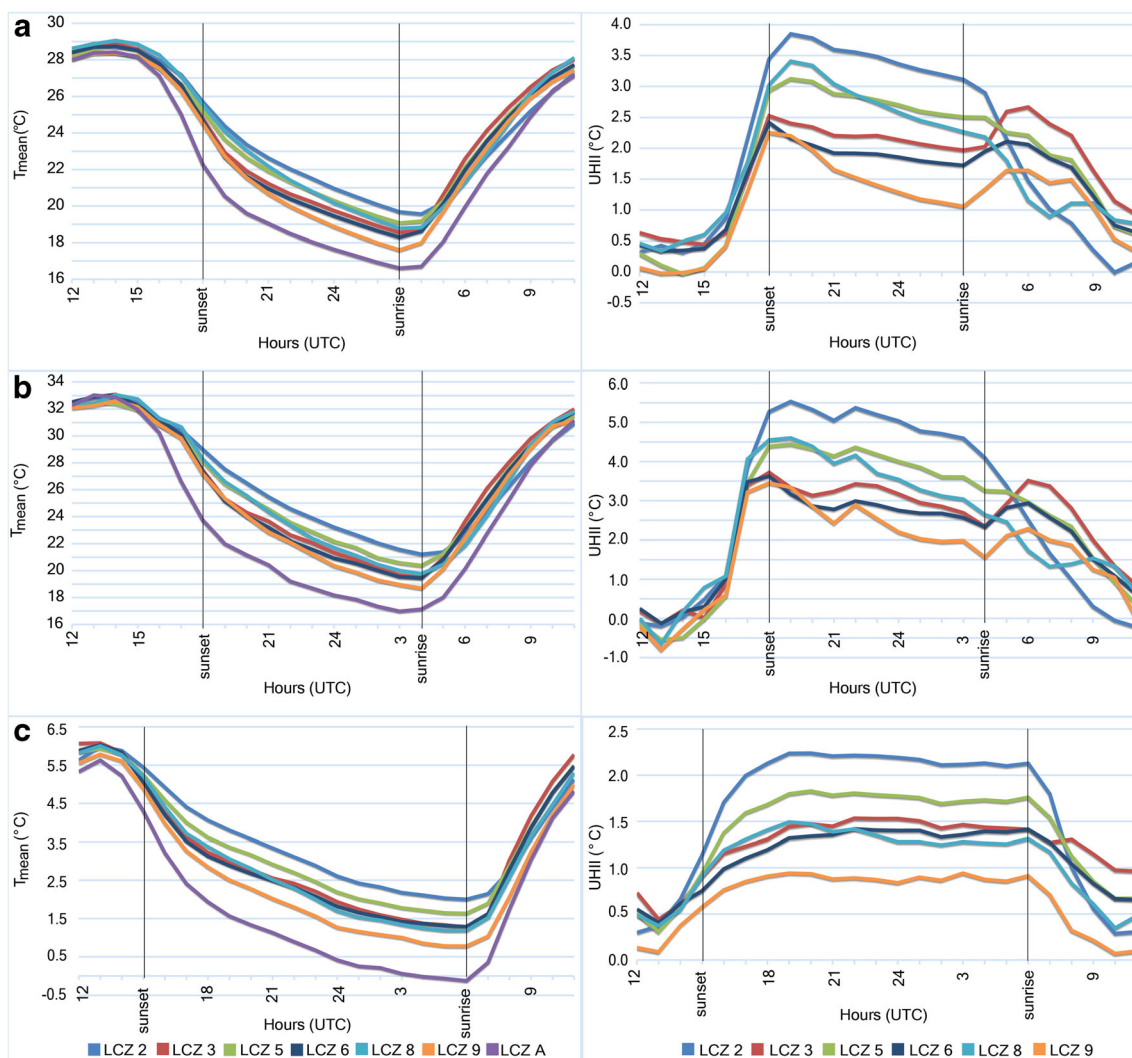


Fig. 5 Hourly changes in T_{mean} (°C) (left) and UHIIs (right) in LCZs during **a** summer, **b** heat wave, and **c** winter

differences obtained between urban and non-urban LCZs in Berlin ($\Delta T_{LCZ5-LCZ B} = 1.5$ °C; Fenner et al. 2014) and Szeged ($\Delta T_{LCZ2-LCZ D} = 0.9$ °C; Skarbit et al. 2017). This is no

surprise, as the representative station for non-urban areas in Novi Sad is in LCZ A, while non-urban station for Berlin and Szeged is in LCZ B and LCZ D, respectively.

Table 3 Daytime and nighttime mean UHII in built LCZs of Novi Sad on seasonal and annual level, and during HW and CW period

		LCZ	2	3	5	6	8	9
UHII _{mean}	Daytime	Winter	0.7	0.9	0.8	0.8	0.6	0.3
		Spring	0.5	0.9	0.7	0.6	0.9	0.4
		Summer	1.0	1.4	1.1	1.1	1.0	0.8
		Autumn	0.7	1.2	0.8	0.9	0.8	0.6
		Annual	0.7	1.1	0.9	0.9	0.8	0.5
		Heat wave	1.3	1.7	1.4	1.5	1.3	1.1
		Cold wave	0.6	1.0	0.8	0.8	0.4	0.2
	Nighttime	Winter	2.1	1.4	1.7	1.3	1.3	0.9
		Spring	2.7	1.7	2.3	1.5	2.4	1.2
		Summer	3.5	2.2	2.8	2.0	2.8	1.6
		Autumn	2.5	1.6	1.9	1.4	1.7	1.1
		Annual	2.6	1.7	2.1	1.5	1.9	1.1
		Heat wave	5.1	3.2	4.1	2.9	3.8	2.6
		Cold wave	2.8	2.3	2.5	2.1	1.9	1.1

The two-phase nocturnal cooling was observed in LCZs. The cooling is more intensive and varies between majority of LCZs during the first cooling phase, while cooling is smaller and similar between LCZs during the second cooling phase. The most intensive cooling is observed in more vegetated and open LCZs A and 9, while the least intensive cooling is observed in more urbanized LCZs 2 and 5. The maximum seasonal CR_{peak} in phase 1 ranged from -1.5 °C in LCZ 2 to -2.8 °C in LCZ A in summer. This is in accordance with summer CR_{peak} obtained in urban (rural) areas of temperate cities: -1 °C h^{-1} (-2.8 °C h^{-1}) in Montreal and -1.5 °C h^{-1} (3 °C h^{-1}) in Vancouver (Oke and Maxwell 1975); -1.8 °C h^{-1} in Mexico City (Jauregui 1986); -1.2 °C h^{-1} in Göteborg (Holmer et al. 2007) and in LCZs 2 and 5 in Nancy (Leconte et al. 2017); and between -1 °C h^{-1} and -2 °C h^{-1} in LCZs of Szeged (Skarbit et al. 2017). More intensive CR_{peak} was observed in Phoenix, ranging from -2.2 °C h^{-1} to -4.9 °C h^{-1} (Chow and Svoma 2011) and in Ouagadougou (Burkina Faso) ranging from -1.9 °C h^{-1} to -5.8 °C h^{-1} (Holmer et al. 2013). In Novi Sad, similarly intensive CR_{peak} were only obtained during HW ranging from -1.6 °C h^{-1} in LCZ 2 to -3.9 °C h^{-1} in LCZ A. Similar CR_{peak} , ranging from -1.5 °C h^{-1} to -3.0 °C h^{-1} , was observed at urban sites in Adelaide during summer nights (Erell and Williamson 2007). CR_{total} , as a new cooling indicator, showed to be the most important indicator of varying cooling signals between LCZs. For example, CR_{total} ranged from -8.1 °C h^{-1} to -10.7 °C h^{-1} between urban LCZs, while it reached -13.5 °C h^{-1} in natural LCZ A during the first cooling phase of HW. An influence of heat accumulation between the start and end of the HW was also noticed, which resulted in more intense CR in LCZs during the second half of the HW. The most noticeable example is LCZ A with daily CR_{peak} ranging from -3.4 °C h^{-1} to -4.3 °C h^{-1} during the first half of HW, and from -4.7 °C h^{-1} to -6.4 °C h^{-1} during the second half of HW. The cooling differences between LCZs were small during phase 2 ($< -0.5\text{ °C h}^{-1}$ for CR_{peak} and CR_{mean}), with similar differences obtained in Göteborg ($< -0.6\text{ °C h}^{-1}$) (Holmer et al. 2007) and in Nancy ($< -0.6\text{ °C h}^{-1}$) (Leconte et al. 2017).

In this study, a general two-phase diurnal heating pattern was noticed. The first heating phase is characterized with intensive LCZ dependent heating with the most intensive HR_{peak} of 3.0 °C h^{-1} in LCZ 8 during HW. At the same time, the least intensive HR_{peak} of 2.0 °C h^{-1} was observed in LCZ 2. In general, it was noticed that HR are dependent on the LCZ with the highest values observed in natural, sparsely built and low-rise areas, while the lowest HR were observed in midrise LCZs 2 and 5 during the first heating phase. For example, the results for Szeged also showed that natural and sparsely built LCZs are warming more rapidly than densely built-up LCZs 2 and 3 (Skarbit et al. 2017). Additionally, Yang et al. (2018) noticed that the warming rates of the open vegetated LCZs (9, D, and A) were significantly larger than in urbanized LCZs in Nanjing (China). Gonçalves et al. (2018) also noticed that the

rural warming was more intensive than the urban warming inside the LCZs of Bragança (Portugal). The HR are smaller during the second heating phase, yet an interesting pattern was noticed: the highest HR were observed in street canyons of LCZ 2, while lower HR were observed in more open LCZs 3 and 5, and in natural LCZ A. Yang et al. (2019) also reported that the urban area had higher HR than rural areas during midday and in early afternoon hours, while the opposite was during the morning hours in Changchun (China).

The most intensive UHI_{mean} was observed between LCZs 2 and A during the nocturnal hours in summer ($\Delta T_{LCZ2-A} = 3.5\text{ °C}$) and HW ($\Delta T_{LCZ2-A} = 5.1\text{ °C}$) due to more intensive cooling in natural areas and less intensive cooling in urban area. Similar $3\text{--}4\text{ °C}$ differences were observed between LCZs 2 and D in Szeged (Skarbit et al. 2017), Nanjing (Yang et al. 2018), Nagano and Uppsala (Stewart et al. 2014), Dublin (Alexander and Mills 2014), and Nancy (Leconte et al. 2015). The absolute maximum hourly T_a differences between built-up LCZs and LCZ A in Novi Sad reached 8 °C in LCZs 2 and 3, followed by 7 °C in LCZs 5 and 8, and 5.5 °C in LCZs 6 and 9 during the nocturnal period of HW. Similar maximum hourly T_a differences are noticed between LCZs 2 and D with 8 °C difference in Nanjing (Yang et al. 2018), 6 °C in Szeged (Unger et al. 2014) and Uppsala (Stewart 2011), and 5 °C in Dublin (Alexander and Mills 2014). At sunrise, UHI swiftly decreases to $< 1\text{ °C}$ due to higher warming in natural areas and lower warming in city.

T_a differences between the stations belonging to the same LCZ were also checked. This was done for LCZs 2, 5, and 6 having 3, 5, and 5 stations, respectively. The results showed that T_{mean} differences between stations belonging to the same LCZ are in most cases negligible with differences $< 0.5\text{ °C}$. Only at one station in each of LCZs 2, 5, and 6, the intra-class thermal differences sometimes exceed 0.5 °C , yet they are always $< 1\text{ °C}$. These small temperature differences among the stations belonging to the same LCZ are likely due to microscale characteristics (e.g., exposure, surface cover; Skarbit et al. 2017), and they indicate that the LCZs of Novi Sad have distinct local climate characteristics. Finally, the present study did not analyze the potential influence of local wind and water sources (e.g., Danube River) on the obtained results.

Conclusion

The long-term T_a analysis revealed that the highest temperatures during nighttime were noticed in urban street canyon in LCZ 2, while the highest temperatures during daytime were noticed in more open, low-rise LCZs 8 and 3. The lowest temperatures were registered in vegetated area outside the city represented by the forest in LCZ A. Seasonal urban-natural differences in T_{min} can reach 3 °C , while intra-urban differences can reach 2.0 °C . Interestingly, the largest differences

were observed during CW when street canyon in LCZ 2 had 5.4 °C higher T_{\min} compared to the forest in LCZ A; during HW, the maximum T_{\min} difference is also between these zones, yet smaller (4.7 °C).

Two-phase nocturnal cooling and two-phase diurnal heating were recognized in LCZs during all investigated periods. The first cooling phase starts at 1–3 h before sunset and lasts until 3–4 h after sunset, and is characterized by LCZ dependent and intensive cooling. The second cooling phase lasts until sunrise and is characterized by LCZ nondependent and less intensive cooling. The most intensive cooling was observed in LCZ A with CR_{peak} of -3.9 °C h^{-1} and CR_{total} of -13.5 °C during first cooling phase of HW. The most urbanized areas (LCZs 2 and 5) had the least intensive cooling. After sunrise, the first heating phase starts and is characterized with intensive LCZ dependent heating with higher HR in natural and low-rise areas and smaller heating in more compact and densely built LCZs due to smaller SVF and higher shadowing effect. The most intensive heating of 3.0 °C h^{-1} was observed in LCZ 8, while the least intensive heating of 2.0 °C h^{-1} was observed in urban canyons in LCZ 2 during HW. The second heating phase starts at 5–8 h after sunrise and is characterized by smaller LCZ nondependent heating until sunset.

As a consequence of varying CR and HR , the most intensive nocturnal UHI was observed in LCZ 2, and the most intensive diurnal UHI was observed in LCZ 3. The absolute maximum hourly UHI of approximately 8 °C was observed in LCZs 2 and 3 when compared to LCZ A during the nocturnal period of HW. On seasonal level, the maximum nocturnal (diurnal) UHI of 3.5 °C (1.4 °C) was observed in LCZ 2 (LCZ 3) during summer.

This research provided a better understanding of T_a dynamics in various built-up neighborhoods of Novi Sad and in a forest outside the city. Methods used in this study can be applied in similar analyses of UHI genesis and dynamics in cities worldwide. The obtained results can contribute to developing the climate-sensitive urban design that could be effective in mitigating UHI effect.

Supplementary Information The online version contains supplementary material available at <https://doi.org/10.1007/s00484-020-02058-w>.

Funding This research has been partly contributed by the Ministry of Education, Science and Technological Development of the Republic of Serbia through the project grant no. 176020.

References

- Alexander P, Mills G (2014) Local climate classification and Dublin's urban heat island. *Atmosfera* 5(4):755–774. <https://doi.org/10.3390/atmos5040755>
- Amfield AJ (2003) Two decades of urban climate research: a review of turbulence, exchanges of energy and water, and the urban heat island. *Int J Climatol* 23(1):1–26. <https://doi.org/10.1002/joc.859>
- Bechtel B, Daneke C (2012) Classification of local climate zones based on multiple earth observation data. *IEEE J Sel Top Appl Earth Obs Remote Sens* 5(4):1191–1202. <https://doi.org/10.1109/JSTARS.2012.2189873>
- Brousse O, Martilli A, Foley M, Mills G, Bechtel B (2016) WUDAPT, an efficient land use producing data tool for mesoscale models? Integration of urban LCZ in WRF over Madrid. *Urban Clim* 17:116–134. <https://doi.org/10.1016/j.uclim.2016.04.001>
- Caluwaerts S, Hamdi R, Top S, Lauwaet D, Berckmans J, Degrauwe D, Dejonghe H, De Ridder K, De Troch R, Duchêne F, Maiheu B (2020) The urban climate of Ghent, Belgium: a case study combining a high-accuracy monitoring network with numerical simulations. *Urban Clim* 31:100565. <https://doi.org/10.1016/j.uclim.2019.100565>
- Chapman L, Muller CL, Young DT, Warren EL, Grimmond CSB, Cai XM, Ferranti EJ (2015) The Birmingham urban climate laboratory: an open meteorological test bed and challenges of the smart city. *Bull Am Meteorol Soc* 96(9):1545–1560. <https://doi.org/10.1175/BAMS-D-13-00193.1>
- Chow WT, Roth, M (2006) Temporal dynamics of the urban heat island of Singapore. *Int J Climatol* 26(15):2243–2260. <https://doi.org/10.1002/joc.1364>
- Chow WT, Svoma BM (2011) Analyses of nocturnal temperature cooling-rate response to historical local-scale urban land-use/land cover change. *J Appl Meteorol Climatol* 50(9):1872–1883. <https://doi.org/10.1175/JAMC-D-10-05014.1>
- Eliasson I (1994) Urban-suburban-rural air temperature differences related to street geometry. *Phys Geogr* 15(1):1–22. <https://doi.org/10.1080/02723646.1994.10642501>
- Erell E, Williamson T (2007) Intra-urban differences in canopy layer air temperature at a mid-latitude city. *Int J Climatol* 27(9):1243–1255. <https://doi.org/10.1002/joc.1469>
- Fenner D, Meier F, Scherer D, Polze A (2014) Spatial and temporal air temperature variability in Berlin, Germany, during the years 2001–2010. *Urban Clim* 10:308–331. <https://doi.org/10.1016/j.uclim.2014.02.004>
- Geletič J, Lehnert M, Dobrovolný P (2016a) Land surface temperature differences within local climate zones, based on two central European cities. *Remote Sens* 8(10):788. <https://doi.org/10.3390/rs8100788>
- Geletič J, Lehnert M, Dobrovolný P (2016b) Modelled spatio-temporal variability of air temperature in an urban climate and its validation: a case study of Brno, Czech Republic. *Hung Geogr Bull* 65(2):169–180. <https://doi.org/10.15201/hungeobull.65.2.7>
- Geletič J, Lehnert M, Savić S, Milošević D (2018) Modelled spatiotemporal variability of outdoor thermal comfort in local climate zones of the city of Brno, Czech Republic. *Sci Total Environ* 624:385–395. <https://doi.org/10.1016/j.scitotenv.2017.12.076>
- Geletič J, Lehnert M, Savić S, Milošević D (2019) Inter-/intra-zonal seasonal variability of the surface urban heat island based on local climate zones in three central European cities. *Build Environ* 156:21–32. <https://doi.org/10.1016/j.buildenv.2019.04.011>
- Gémes O, Tobak Z, Van Leeuwen B (2016) Satellite based analysis of surface urban heat island intensity. *J Environ Geogr* 9(1–2):23–30. <https://doi.org/10.1515/jengeo-2016-0004>
- Gholami RM, Beck C (2019) Towards the determination of driving factors of varying LST-LCZ relationships: a case study over 25 cities. *Geogr Pannon* 23(4):289–307. <https://doi.org/10.5937/gp23-24238>
- Giannopoulou K, Santamouris M, Livada I, Georgakis C, Caouris Y (2010) The impact of canyon geometry on intra urban and urban: suburban night temperature differences under warm weather conditions. *Pure Appl Geophys* 167(11):1433–1449. <https://doi.org/10.1007/s00024-010-0099-8>
- Gonçalves A, Omellas G, Castro Ribeiro A, Maia F, Rocha A, Feliciano M (2018) Urban cold and heat island in the city of Bragança (Portugal). *Climate* 6(3):70. <https://doi.org/10.3390/cli6030070>

- Haeger-Eugensson M, Holmer B (1999) Advection caused by the urban heat island circulation as a regulating factor on the nocturnal urban heat island. *Int J Climatol* 19(9):975–988. [https://doi.org/10.1002/\(SICI\)1097-0088\(199907\)19:9<975::AID-JOC399>3.0.CO;2-J](https://doi.org/10.1002/(SICI)1097-0088(199907)19:9<975::AID-JOC399>3.0.CO;2-J)
- Holmer B, Thorsson S, Eliasson I (2007) Cooling rates, sky view factors and the development of intra-urban air temperature differences. *Geogr Ann A* 89(4):237–248. <https://doi.org/10.1111/j.1468-0459.2007.00323.x>
- Holmer B, Thorsson S, Lindén J (2013) Evening evapotranspirative cooling in relation to vegetation and urban geometry in the city of Ouagadougou, Burkina Faso. *Int J Climatol* 33(15):3089–3105. <https://doi.org/10.1002/joc.3561>
- Jauregui E (1986) The urban climate of Mexico City. Urban climatology and its applications with special regard to tropical areas. World Climate Programme, WMO Publication No. 652, World Meteorological Organisation, Geneva, pp 63–86
- Johnson DB (1985) Urban modification of diurnal temperature cycles in Birmingham, UK. *J Climatol* 5(2):221–225. <https://doi.org/10.1002/joc.3370050208>
- Konarska J, Holmer B, Lindberg F, Thorsson S (2016) Influence of vegetation and building geometry on the spatial variations of air temperature and cooling rates in a high-latitude city. *Int J Climatol* 36(5):2379–2395. <https://doi.org/10.1002/joc.4502>
- Kotharkar R, Bagade A, Agrawal A (2019) Investigating local climate zones for outdoor thermal comfort assessment in an Indian city. *Geogr Pannon* 23(4):318–328. <https://doi.org/10.5937/gp23-24251>
- Kottek M, Grieser J, Beck C, Rudolf B, Rubel F (2006) World map of the Köppen–Geiger climate classification updated. *Meteorol Z* 15(3):259–263. <https://doi.org/10.1127/0941-2948/2006/0130>
- Kovács A, Németh Á (2012) Tendencies and differences in human thermal comfort in distinct urban areas in Budapest, Hungary. *Acta Climatol Chorol* 46:115–124
- Leconte F, Bouyer J, Claverie R, Pétrissans M (2015) Using local climate zone scheme for UHI assessment: evaluation of the method using mobile measurements. *Build Environ* 83:39–49. <https://doi.org/10.1016/j.buildenv.2014.05.005>
- Leconte F, Bouyer J, Claverie R, Pétrissans M (2017) Analysis of nocturnal air temperature in districts using mobile measurements and a cooling indicator. *Theor Appl Climatol* 130(1–2):365–376. <https://doi.org/10.1007/s00704-016-1886-7>
- Lee DO (1979) Contrasts in warming and cooling rates at an urban and a rural site. *Weather* 34(2):60–66. <https://doi.org/10.1002/j.1477-8696.1979.tb03406.x>
- Lee SH, Baik JJ (2010) Statistical and dynamical characteristics of the urban heat island intensity in Seoul. *Theor Appl Climatol* 100(1–2):227–237. <https://doi.org/10.1007/s00704-009-0247-1>
- Lehnert M, Geletič J, Husák J, Vysoudil M (2015) Urban field classification by “local climate zones” in a medium-sized central European city: the case of Olomouc (Czech Republic). *Theor Appl Climatol* 122(3–4):531–541. <https://doi.org/10.1007/s00704-014-1309-6>
- Lehnert M, Kubeček J, Geletič J, Jurek M, Frajer J (2018) Identifying hot and cool spots in the city centre based on bicycle measurements: the case of Olomouc, Czech Republic. *Geogr Pannon* 22(4):230–240. <https://doi.org/10.5937/gp22-19750>
- Lelovics E, Unger J, Gál T, Gál CV (2014) Design of an urban monitoring network based on local climate zone mapping and temperature pattern modelling. *Clim Res* 60(1):51–62. <https://doi.org/10.3354/cr01220>
- Lelovics E, Unger J, Savić S, Gál TM, Milošević D, Gulyás Á, Marković V, Arsenović D, Gál CV (2016) Intra-urban temperature observations in two central European cities, a summer study. *Időjárás* 120(3):283–300
- Middel A, Hüb K, Brazel AJ, Martin CA, Guhathakurta S (2014) Impact of urban form and design on mid-afternoon microclimate in Phoenix local climate zones. *Landscape Urban Plan* 122:16–28. <https://doi.org/10.1016/j.landurbplan.2013.11.004>
- Milošević DD, Savić SM, Marković V, Arsenović D, Šećerov I (2016) Outdoor human thermal comfort in local climate zones of Novi Sad (Serbia) during heat wave period. *Hung Geogr Bull* 65(2):129–137. <https://doi.org/10.15201/hungeobull.65.2.4>
- Nakamura Y, Oke TR (1988) Wind, temperature and stability conditions in an east–west oriented urban canyon. *Atmos Environ* 22:2691–2700. [https://doi.org/10.1016/0004-6981\(88\)90437-4](https://doi.org/10.1016/0004-6981(88)90437-4)
- Oke TR, East C (1971) The urban boundary layer in Montreal. *Bound-Layer Meteorol* 1(4):411–437. <https://doi.org/10.1007/BF00184781>
- Oke TR, Maxwell GB (1975) Urban heat island dynamics in Montreal and Vancouver. *Atmos Environ* 9(2):191–200. [https://doi.org/10.1016/0004-6981\(75\)90067-0](https://doi.org/10.1016/0004-6981(75)90067-0)
- Oke TR, Mills G, Christen A, Voogt JA (2017) *Urban climates*. Cambridge University Press, Cambridge
- Perera NGR, Emmanuel R (2018) A “local climate zone” based approach to urban planning in Colombo, Sri Lanka. *Urban Clim* 23:188–203. <https://doi.org/10.1016/j.uclim.2016.11.006>
- Puliafito SE, Bochaca FR, Allende DG, Fernandez RP (2013) Green areas and microscale thermal comfort in arid environments: a case study in Mendoza, Argentina. *Atmos ClimSci* 3(3):372–384. <https://doi.org/10.4236/acs.2013.33039>
- Savić S, Marković V, Šećerov I, Pavić D, Arsenović D, Milošević D, Dolinaj D, Nagy I, Pantelić M (2018) Heat wave risk assessment and mapping in urban areas: case study for a mid-sized central European city, Novi Sad (Serbia). *Nat Hazards* 91(3):891–911. <https://doi.org/10.1007/s11069-017-3160-4>
- Šećerov I, Savić S, Milošević D, Marković V, Bajšanski I (2015) Development of an automated urban climate monitoring system in Novi Sad (Serbia). *Geogr Pannon* 19(4):174–183. <https://doi.org/10.5937/GeoPan1504174S>
- Šećerov I, Dolinaj D, Pavić D, Milošević D, Savić S, Popov S, Živanov Ž (2018) Environmental monitoring systems: review and future development. *Wirel Eng Technol* 10(1):1–18. <https://doi.org/10.4236/wet.2019.101001>
- Šećerov IB, Savić SM, Milošević DD, Arsenović DM, Dolinaj DM, Popov SB (2019) Progressing urban climate research using a high-density monitoring network system. *Environ Monit Assess* 191(2):89. <https://doi.org/10.1007/s10661-019-7210-0>
- Siu LW, Hart MA (2013) Quantifying urban heat island intensity in Hong Kong SAR, China. *Environ Monit Assess* 185(5):4383–4398. <https://doi.org/10.1007/s10661-012-2876-6>
- Skarbit N, Gal T, Unger J (2015). Airborne surface temperature differences of the different local climate zones in the urban area of a medium sized city. In: 2015 Joint Urban Remote Sensing Event (JURSE). IEEE, Lausanne, Switzerland, pp 1–4. <https://doi.org/10.1109/JURSE.2015.7120497>
- Skarbit N, Stewart ID, Unger J, Gál T (2017) Employing an urban meteorological network to monitor air temperature conditions in the ‘local climate zones’ of Szeged, Hungary. *Int J Climatol* 37:582–596. <https://doi.org/10.1002/joc.5023>
- Stewart ID (2011) A systematic review and scientific critique of methodology in modern urban heat island literature. *Int J Climatol* 31(2):200–217. <https://doi.org/10.1002/joc.2141>
- Stewart ID, Oke TR (2012) Local climate zones for urban temperature studies. *Bull Am Meteorol Soc* 93(12):1879–1900. <https://doi.org/10.1175/BAMS-D-11-00019.1>
- Stewart ID, Oke TR, Krayenhoff ES (2014) Evaluation of the ‘local climate zone’ scheme using temperature observations and model simulations. *Int J Climatol* 34(4):1062–1080. <https://doi.org/10.1002/joc.3746>
- Unger J, Savić S, Gál T (2011) Modelling of the annual mean urban heat island pattern for planning of representative urban climate station network. *Adv Meteorol* 2011:1–9. <https://doi.org/10.1155/2011/398613>

- Unger J, Lelovics E, Gál T (2014) Local climate zone mapping using GIS methods in Szeged. *Hung Geogr Bull* 63(1):29–41. <https://doi.org/10.15201/hungeobull.63.1.3>
- Unger J, Skarbit N, Gál T (2018) Evaluation of outdoor human thermal sensation of local climate zones based on long-term database. *Int J Biometeorol* 62(2):183–193. <https://doi.org/10.1007/s00484-017-1440-z>
- WMO (2008) Guide to meteorological instruments and methods of observation. 7th ed. WMO Instruments and Observing Methods Rep. WMO-8, 681 pp. [Available online at <https://www.weather.gov/media/epz/mesonet/CWOP-WMO8.pdf>]. Accessed 9 Sept 2020
- Yang X, Yao L, Jin T, Peng LL, Jiang Z, Hu Z, Ye Y (2018) Assessing the thermal behavior of different local climate zones in the Nanjing metropolis, China. *Build Environ* 137:171–184. <https://doi.org/10.1016/j.buildenv.2018.04.009>
- Yang C, Wang R, Zhang S, Ji C, Fu X (2019) Characterizing the hourly variation of urban heat islands in a snowy climate city during summer. *Int J Environ Res Public Health* 16(14):2467. <https://doi.org/10.3390/ijerph16142467>